Journal of Magnetic Resonance 200 (2009) 214–225

Contents lists available at ScienceDirect

Journal of Magnetic Resonance

journal homepage: www.elsevier.com/locate/jmr

Observation of restricted diffusion in the presence of a free diffusion compartment: Single- and double-PFG experiments

Noam Shemesh [a], Evren Özarslan [b], Amnon Bar-Shir [a], Peter J. Basser [b], Yoram Cohen [a,*]

[a] School of Chemistry, The Raymond and Beverly Sackler Faculty of Exact Sciences, Tel Aviv University, Israel
[b] Section on Tissue Biophysics and Biomimetics, NICHD, National Institutes of Health, Bethesda, MD, USA

ARTICLE INFO

Article history:
Received 25 May 2009
Revised 2 July 2009
Available online 9 July 2009

Keywords:
Double-pulsed gradient spin echo
PGSE
Double PGSE
d-PGSE
Diffusion
White matter phantom
Crossing fibers
Low-*q*
Pulsed field gradients
PFG
NMR
Fast
Slow diffusing

ABSTRACT

Theoretical and experimental studies of restricted diffusion have been conducted for decades using single pulsed field gradient (s-PFG) diffusion experiments. In homogenous samples, the diffusion–diffraction phenomenon arising from a single population of diffusing species has been observed experimentally and predicted theoretically. In this study, we introduce a composite bi-compartmental model which superposes restricted diffusion in microcapillaries with free diffusion in an unconfined compartment, leading to fast and slow diffusing components in the NMR signal decay. Although simplified (no exchange), the superposed diffusion modes in this model may exhibit features seen in more complex porous materials and biological tissues. We find that at low *q*-values the freely diffusing component masks the restricted diffusion component, and that prolongation of the diffusion time shifts the transition from free to restricted profiles to lower *q*-values. The effect of increasing the volume fraction of freely diffusing water was also studied; we find that the transition in the signal decay from the free mode to the restricted mode occurs at higher *q*-values when the volume fraction of the freely diffusing water is increased. These findings were then applied to a phantom consisting of crossing fibers, which demonstrated the same qualitative trends in the signal decay. The angular d-PGSE experiment, which has been recently shown to be able to measure small compartmental dimensions even at low *q*-values, revealed that microscopic anisotropy is lost at low *q*-values where the fast diffusing component is prominent. Our findings may be of importance in studying realistic systems which exhibit compartmentation.

1. Introduction

Diffusion NMR is widely used as a non-invasive probe in a multitude of applications ranging from characterization of chemical moieties in solution to inferring micro-structural features in porous materials, rocks, and biological tissue [1–8]. Most diffusion NMR methods employ single-pulsed gradient spin echo (s-PGSE) or pulsed gradient stimulated echo (s-PGSTE) methodologies, which are based on spin echo or stimulated echo sequences containing a pair of diffusion sensitizing pulsed gradient vectors, **G**, with duration δ, that are separated by the diffusion time, Δ [9,10]. The spatial encoding of the nuclei by these pulsed gradients results in dephasing of spins due to translational motion, leading to an attenuation of the NMR echo signal. The diffusion-driven signal attenuation can be used to infer molecular and micro-structural characteristics of the diffusing species and its surroundings by examining the spatial and temporal dependence of the self-diffusion coefficient, D [8]. In freely diffusing systems, where the molecules are not hampered by barriers, the logarithm of the signal decay is linearly dependent on the b-value, from which D can be extracted (where $(2\pi|\mathbf{q}|)^2 t_d$, and $\mathbf{q} = (2\pi)^{-1}\gamma\delta\mathbf{G}$, t_d is the diffusion time and is equal to $(\Delta - \delta/3)$ in case of rectangular pulsed field gradients) [11]. In isotropic systems, D is invariant to rotation, and the same linear attenuation will be observed regardless of the orientation of the gradients [11]. Moreover, examining the time dependence of D in freely diffusing systems reveals that D is independent of the diffusion time; consequently, the root mean-squared displacement (rmsd) increases linearly with $t_d^{1/2}$. Both the linear decay of the logarithm of the NMR signal as a function of the b-value and the linear dependence of the mean squared displacements on t_d demonstrate the Gaussian nature of free diffusion, while the directional independence of the signal decay implies on isotropy of the diffusing medium (non-restricting in any direction). This can be regarded as a free diffusion profile.

A completely different displacement profile is obtained when the diffusing molecules are confined by impermeable boundaries forming a restricted compartment. Here, the logarithm of the signal attenuation deviates from linearity with increasing b-value. In these cases, and by contrast to a free diffusion profile, D is time

* Corresponding author. Address: School of Chemistry, The Raymond and Beverly Sackler Faculty of Exact Sciences, Tel Aviv University, Ramat Aviv, Tel Aviv 69978, Israel. Fax: +972 3 6407469.
E-mail address: ycohen@post.tau.ac.il (Y. Cohen).

1090-7807/$ - see front matter © 2009 Elsevier Inc. All rights reserved.
doi:10.1016/j.jmr.2009.07.005

dependent: it has been shown that for short Δ, a free diffusion profile is obtained and the rmsd increases linearly when plotted against $\Delta^{1/2}$, due to the very small fraction of molecules that experience the boundaries [8,11]. When Δ is prolonged, the pore is gradually sampled by more and more molecules, resulting in a deviation from linearity which characterizes restricted diffusion, a property that can be used to extract structural information characterizing the pores. Notably, when the pores are of the same size, and Δ is sufficiently long to probe the boundaries of the restricting compartment, a non-monotonic profile, manifested in diffusion–diffractions, is observed when the NMR signal decay is plotted against the wave-vector $\mathbf{q}$ [11–13]. The size of the pore can be derived from the diffusion–diffraction troughs; when the pores are anisotropic, the diffusion–diffraction patterns have a strong dependence on the rotational angle between the principal axis of the pore and the orientation of the gradients, affording information about pore geometry [12,14–17]. In recent years, the theoretical background for such phenomena has been advanced for various geometries [18–21], and these NMR diffusion–diffractions were observed experimentally in systems which are characterized by pores with relatively monodisperse pore sizes [13–15,17,22]. In cases where the diffraction troughs disappear due to susceptibility effects induced by inhomogeneities of the sample, it has been shown that by using radiofrequency (RF) gradients [23,24] or bipolar gradients [25] one can recover the diffraction-like features, and therefore extract the structural information from the sample. The q-space approach, which makes use of the Fourier relation between the signal decay and the average propagator, $\bar{P}$ [26], provides similar structural information from samples that show shallow diffusion–diffraction troughs, or even no diffusion–diffraction troughs whatsoever, (e.g. due to size distributions in the sample) such as red blood cells [27] and even nerve tissue [1,28–32], respectively.

For each of the diffusion modes mentioned above, i.e., free and restricted diffusion, the signal decay is characterized by its distinctive diffusion profile. However, many real-world systems that have either non-exchanging or slowly exchanging compartments, in which each compartment has a distinctive apparent diffusion coefficient (ADC), and the signal decay exhibits a superposition of the diffusion modes. For instance, in white matter, where both intra and extracellular water contribute to the signal decay within the same voxel, a signal decay which is non-mono-exponential is observed [1,26,28,32–36]. Another example is porous media, where a freely diffusing solvent in the bulk will have a higher ADC compared to the molecules that are confined within the pores and undergo restricted diffusion. Other systems which may be pertinent in this context include crossing fibers in biological tissue, partial volume contributions of free water from CSF in nerve bundles, and, to a certain extent, intra- and extra-cellular water, all of which exhibit non-mono-exponential signal decay due to the presence of multiple compartments.

Despite there being multiple compartments in nerves, diffusion tensor imaging (DTI) conducted at low b-values produces a single, voxel-averaged diffusion tensor [11,37]. The fast diffusing component can be suppressed while the slowly diffusing component is more significantly expressed by using the q-space approach, which employs high b-values. Doing so may provide useful information about microstructural features, because the slowly diffusing component may be a better reporter for white matter tissue [1,16,29–32].

Very recently, double pulsed field gradient (d-PFG) experiments [38] have been gaining increasing attention due to their ability to overcome some limitations of s-PFG. For example, d-PFG reveals microscopic anisotropy in macroscopically isotropic samples [39–41], thus providing a signature for restricted diffusion in small compartments, even at low q-values [42–44]. The d-PGSE sequence, shown in Fig. 1A, contains two diffusion sensitizing gradient pairs, $\mathbf{G}_1$ and $\mathbf{G}_2$ with durations, δ_1 and δ_2 for each individual gradient, $\mathbf{G}_1$ and $\mathbf{G}_2$, respectively. The gradient pairs are separated by a mixing time (t_m). Note that in the d-PGSE experiment, two diffusion times Δ_1 and Δ_2 exist during which the spins can diffuse. The corresponding $\mathbf{q}$ vectors for the two encoding times can be taken to have the same magnitude, i.e. $q = |\mathbf{q}_1| = |\mathbf{q}_2|$, where $\mathbf{q_i} = (2\pi)^{-1}\gamma\delta\mathbf{G_i}$. The d-PGSE sequence was first proposed in 1990 by Cory et al. [38], and was initially used for one- and two-dimensional characterization of porous materials [45–47], for suppression of convection artifacts [48], and for studying flow phenomena [49]. The potential of the d-PGSE experiment to reveal microscopic anisotropy in systems characterized by macroscopic isotropy was demonstrated on lyotropic liquid crystals [39]. These findings were then extended to a gray matter phantom and fixed gray matter [40], and finally to excised spinal cord [41]. A recent theoretical study regarding the signal decay in multiple-PGSE experiments, and d-PGSE particularly, predicted rather peculiar phenomena of zero crossings of the signal in confined geometries (negative diffractions) [50]. These predictions were corroborated experimentally, and the dependence of the signal decay on the experimental parameters in d-PGSE experiments was demonstrated [51]. Owing to the actual zero crossing, it was shown that, as predicted, the negative diffractions are more robust to variations in pore size distributions, and variation in the q-value of diffractions with prolongation of the mixing times and other experimental parameters was observed [51].

A theoretical study published by Mitra in 1995 suggested that performing the angular d-PGSE experiment in confined geometries using low q-values should yield an angular dependence of the signal from which the compartment size may be calculated [52]. Although Mitra's study was conducted in a limiting case in which $\Delta \to \infty$, $\delta \to 0$, and $t_m \to 0$ or $t_m \to \infty$, it suggested a new tool for measuring sizes of small compartments using relatively weak gradients, which could be clinically feasible. The angular dependence of the signal decay at short t_m is a measure of the microscopic anisotropy induced by the boundaries of the restricting compartment from which the compartment size may be extracted even at low q-values. A new general theoretical treatment of diffusion in d-PGSE experiments, both at low q and at higher q-values was recently proposed [42,43], and the predicted angular dependence was corroborated experimentally. As demonstrated by these studies, this new theoretical framework can account for variation of every experimental parameter one could specify in a d-PGSE sequence [43,44]. A second variant of the d-PGSE sequence, (shown in Fig. 1B) was also introduced in which the two inner gradients (the second $\mathbf{G}_1$ and the first $\mathbf{G}_2$) are superposed, so that t_m is effectively 0—a desirable condition for enhancing the angular dependence.

Although the superposition of two diffusion modes and the effects of compartmentation on the signal decay has been investigated theoretically in several studies [53,54], the effect of adding another compartment to a system which already exhibits diffusion–diffraction patterns has never been studied. In this study, we sought to investigate the signal decay and the structural information that can be extracted thereof, using a novel phantom that simultaneously exhibits two diffusion modes: free diffusion and restricted diffusion. To that end, we employ a composite bi-compartmental phantom, which consists of a fast diffusion compartment (FDC) and a slow diffusion compartment (SDC) comprised of free water and water in restricted impermeable microcapillaries, respectively. In the FDC, barriers for diffusion are not present and the water is not confined to any particular geometry; therefore the water undergoes free diffusion. In the SDC, the barriers imposed by the walls of the microcapillaries allow restricted diffusion to occur, when diffusion is not measured parallel to the main axis

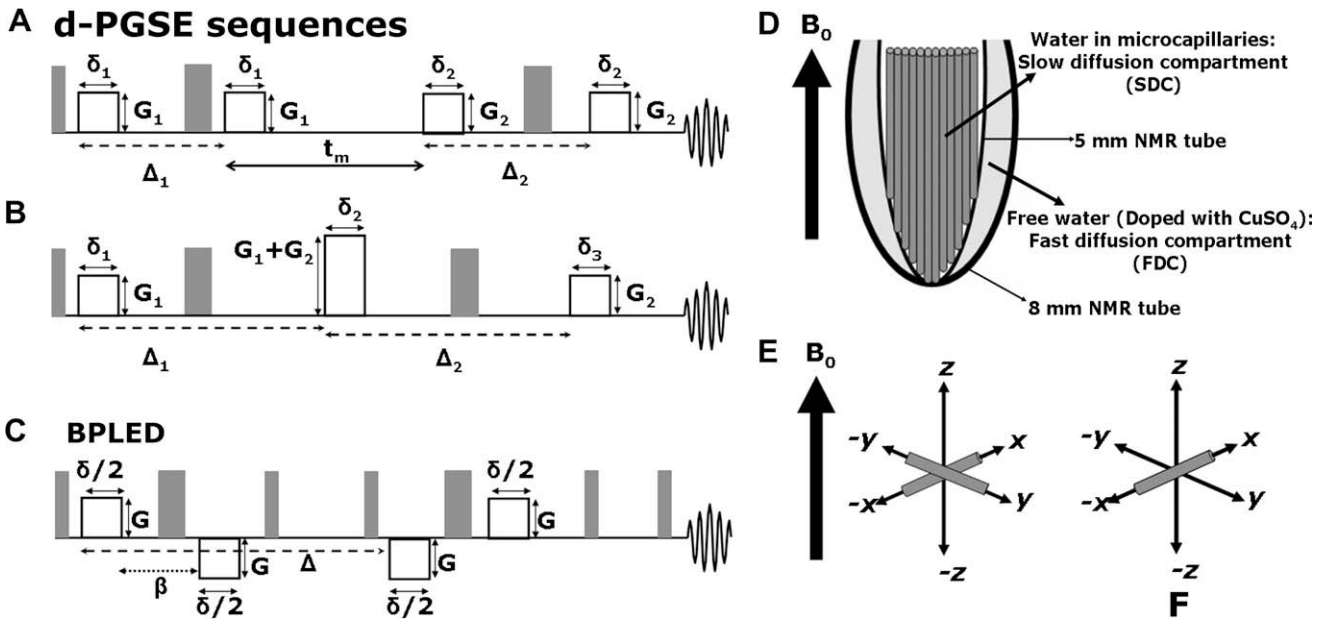

Fig. 1. Sequences and phantoms. (A) d-PGSE sequence, defining the diffusion times, Δ_1 and Δ_2, the mixing time (t_m), and the gradients $\mathbf{G}_1$ and $\mathbf{G}_2$ and their durations (δ_1 and δ_2, respectively). (B) The d-PGSE variant used in this study. Note that the $\mathbf{G}_1$ and $\mathbf{G}_2$ were superposed, rendering the mixing time effectively 0. (C) The bi-polar LED (BPLED) sequence, used for the crossing fibers phantom. Note the duration β, which is referred to in-text. (D) Cartoon of the bi-compartmental phantom. Note that the water diffusing freely in the free diffusion compartment (FDC) is separated from the microcapillaries. The microcapillaries serve as the slow diffusion compartment (SDC). The 4 mm sleeve is not shown for convenience. (E) The crossing fibers phantom, in which two bundles of microcapillaries were aligned with their main axis perpendicular to each other, and to the main magnetic field. (F) The phantom in which one of the crossing bundles was removed, to measure the decay in the presence of only a single compartment.

of the microcapillaries. The two compartments are completely isolated from each other. The advantage of such a phantom is that it is well controlled and the "ground truth" is known; the structure, geometry and orientation of the microcapillaries in the SDC is well-known *a-priori*, as well as the diffusion coefficient of the free water in the FDC. Therefore, in such a phantom the free water in the FDC and restricted water in the SDC give rise to fast and slow diffusing components in the NMR signal decay respectively, and we are able to reliably investigate the way in which signal from the FDC affects the signal from the SDC at different values of q, and compare the theoretical predictions to the experimental results. Using the bi-compartmental phantom, we could also test, for the first time, how the properties revealed by the d-PGSE experiment are affected by the presence of the two diffusion modes at different q-values, and investigate the structural information that can be extracted in such cases. Another point that is addressed in this study relates to the comparison of d- and s-PGSE experiments. When a single compartment exists, comparing the s- and d-PGSE sequences can easily be done by scaling the q-values such that the diffusion curves nicely fit and the same structural information is obtained [44,50]. The question of how to compare s-PGSE and d-PGSE data when two diffusion modes co-exist, as in our bi-compartmental phantom, and indeed, in real systems, is also tackled in this study.

2. Materials and methods

All measurements were performed on a Bruker 8.4 T NMR spectrometer using a Micro5 probe capable of producing nominal pulsed gradients up to 190 G/cm in each direction. The crossing fibers experiment was performed using a mini-imaging (Mini 5) probe capable of producing pulsed gradients up to 20 G/cm in each direction. Hollow microcapillaries with nominal inner diameters (ID) of 10 ± 1, 19 ± 1, or 48 ± 1 μm (Polymicro Technologies, Phoenix, AZ, USA) were immersed in water for several days, prior to each experiment.

2.1. Bi-compartmental phantom construction

Fig. 1D shows a cartoon of the bi-compartmental phantom. Freely diffusing water in the FDC undergoes Gaussian (free) diffusion while water in the microcapillaries experiences restricted diffusion forming the SDC of the bi-compartmental phantom. The microcapillaries were packed into a 4 mm glass sleeve (not shown in Fig. 1D) which was inserted into a 5 mm NMR tube, aligned with the main axis parallel to the z-direction of the magnet. The 5 mm NMR tube was then inserted to an 8 mm NMR tube with the main axis parallel to the z-direction of the magnet. The 8 mm NMR tube was filled with 1 ml of D_2O (D-Chem, Israel) to which 5 μl of 200 mM $CuSO_4$ solution (Sigma–Aldrich, Israel) was added. To achieve larger amounts of pure H_2O in the FDC, water content was increased by adding water to the mixture. Typical linewidths of 5–15 Hz were obtained after shimming.

2.2. MR experiments

2.2.1. Relaxation experiments

Relaxation rates T_1 and T_2 of each compartment were separately measured using the inversion recovery and Carr–Purcell–Meiboom–Gill (CPMG) sequences, respectively. To measure the relaxation rates of the water in the SDC, H_2O-filled microcapillaries with a nominal ID of 10 ± 1 μm were used. To measure the relaxation rates of the FDC, we used a sample consisting of 1 ml D_2O to which 20 μl of water doped with $CuSO_4$ was added, such that the final $CuSO_4$ concentration was 1 mM.

2.2.2. Signal decay in the presence of two components

For this set of experiments, microcapillaries with ID of 10 ± 1 μm were used as the SDC and 20 μl of water in 1 ml of D_2O in the FDC. For the x-direction, s-PGSE experiments were conducted with the following parameters: 48 q-values were collected with Δ/δ = 30/3 ms and G_{max} of 160 G/cm resulting in a q_{max} of 2043 cm^{-1}. The number of scans was set to 16. For the z-direction,

8 q-values were collected with Δ/δ = 30/3 ms and G_{max} of 40 G/cm, resulting in a q_{max} of 510 cm^{-1}, and with NS = 16.

2.2.3. Dependence of the signal decay on the diffusion time

For this set of experiments, microcapillaries with ID of 19 ± 1 μm were used with 80 μl of water in 1 ml of D_2O in the FDC. s-PGSE measurements were performed with gradients applied in the x-direction with the following parameters: 48 q-values were collected with G_{max} of 160 G/cm and with δ = 2 ms, resulting in a q_{max} of 1362 cm^{-1}. The diffusion time Δ was varied between 4 and 200 ms, and with NS = 16.

2.2.4. Dependence of the signal decay on the amount of water in the FDC

To test the effect of increasing the amount of freely diffusing water on the signal decay, we first measured the diffusion profile of the microcapillaries, without water in the FDC. Microcapillaries with ID of 19 ± 1 μm were first measured by the s-PGSE using the following parameters: 48 q-values were collected with G_{max} of 160 G/cm and with Δ/δ = 100/2 ms, resulting in a q_{max} of 1362 cm^{-1} and with NS = 16. The same microcapillaries were then placed in the bi-compartmental phantom. To form the FDC, 1 ml of D_2O were added containing 20 or 100 μl of water was added to the 8 mm NMR tube (Fig. 1D). The s-PGSE measurement was conducted in the x-direction with the following parameters: 48 q-values were collected with G_{max} of 120 G/cm and δ = 2 ms resulting in a q_{max} of 1022 cm^{-1} and with Δ = 100 or 200 ms. The number of scans was set to 16.

2.2.5. Crossing fibers phantom

The crossing fibers phantom was described in detail in [25]. Briefly, a bundle of water-filled microcapillaries with ID = 48 ± 1 μm were aligned with their main axis parallel to the x-direction. Another bundle of microcapillaries with the same ID was aligned with the main axis along the y-direction, such that the main axis of the fibers was perpendicular to that of the fibers in the x-direction (Fig. 1E). Since the crossing fibers sample suffers from susceptibility artifacts [25], the bi-polar LED (BPLED) sequence [55] was used. The BPLED measurement was conducted in the x-direction with the following parameters: 23 q-values were collected with G_{max} of 16 G/cm and with Δ/δ = 1000/10 ms, resulting in a q_{max} of 681 cm^{-1}. The same measurement was conducted for the phantom in which the fiber bundle aligned with its main axis in the x-direction was removed, leaving only one bundle with its main axis along the y-direction. The single bundle served as a control experiment for the signal decay in the presence of only one component (Fig. 1F). For these experiments, NS = 224.

2.2.6. d-PGSE experiments in the bi-compartmental model

The d-PGSE sequence is described in detail in references [44,51]. In the present study, the variant of the d-PGSE sequence in which the mixing time (t_m) is zero was used (Fig. 1B). In this study, the two gradient vectors were always equal, i.e., $\mathbf{G}_1 = \mathbf{G}_2$, and the results are plotted as a function of q, where $q = q_1 = q_2$. The bi-compartmental phantom was constructed with 19 ± 1 μm microcapillaries as the SDC. To test the effect of amount of water in the FDC, 20 or 100 μl of water in 1 ml of D_2O were added to the FDC; to test the effect of prolonging the diffusion times, two diffusion times were measured for each concentration of water. The d-PGSE measurement was performed with both gradient pairs in the x-direction, i.e., $\varphi = 0°$, with the following parameters: 32 q-values were collected with G_{max} of 60 G/cm and with $\delta_1 = \delta_2 = \delta_3$ = 2 ms, resulting in a q_{max} of 510 cm^{-1} and with diffusion times $\Delta_1 = \Delta_2$ = 100 or 200 ms, and with NS = 16.

2.2.7. Comparing d-PGSE and s-PGSE experiments

To compare the d-PGSE and s-PGSE, a bi-compartmental phantom was constructed with 19 ± 1 μm microcapillaries as the SDC and 100 μl of water in 1 ml of D_2O in the FDC. The s-PGSE measurement was performed with the following parameters: 48 q-values were collected with G_{max} of 120 G/cm and with Δ/δ = 200/2 ms, resulting in a q_{max} of 1022 cm^{-1} and with NS = 16. The d-PGSE measurement was conducted in the x-direction for both gradient pairs, i.e., $\varphi = 0°$, with the following parameters: 48 q-values were collected with G_{max} of 60 G/cm and with $\delta_1 = \delta_2 = \delta_3$ = 2 ms, resulting in a q_{max} of 510 cm^{-1} and with diffusion times $\Delta_1 = \Delta_2$ = 200 ms and with NS = 16. The data are plotted against q for the s-PGSE results, and against $2q$ or $2^{1/2}q$ for d-PGSE results. The data for d-PGSE experiments is magnitude calculated to be able to present the negative diffraction on the logarithmic scale.

2.2.8. Angular d-PGSE experiments in the bi-compartmental phantom

The angular d-PGSE experiment is described in detail in reference [44]. Briefly, the experiment is performed in the following manner: $\mathbf{G}_1$ is fixed along the x-axis throughout the experiment, and the orientation of $\mathbf{G}_2$ is varied in the x–y plane along the azimuthal angle between $\mathbf{G}_1$ and $\mathbf{G}_2$, φ. Microcapillaries with ID of 19 ± 1 μm were used in the bi-compartmental phantom in the SDC and 20 μl of water in 1 ml of D_2O were added in the FDC. For this set of experiments, the d-PGSE measurement was conducted for 24 different values of φ between $\varphi = 0°$ and 360°. The following parameters were used: 16 q-values were collected with G_{max} of 35 G/cm and with $\delta_1 = \delta_2 = \delta_3$ = 2 ms, resulting in a q_{max} of 298 cm^{-1} and with diffusion times $\Delta_1 = \Delta_2$ = 100 or 200 ms. The number of scans was set to 16.

2.3. Theoretical analysis

Because the water within the bi-compartmental composite phantoms is non-exchanging, the NMR signal can be written as the sum of two expressions, i.e.,

$$S(\mathbf{q}) = S_{free}E_{free}(\mathbf{q}) + S_{rest}E_{rest}(\mathbf{q}).$$

Here, the second term results from diffusion taking place within the microcapillaries and the first term is due to water molecules diffusing between the two NMR tubes. $E_{free}(\mathbf{q})$ and $E_{rest}(\mathbf{q})$ are the NMR signal attenuations that are equal to unity when $|\mathbf{q}| = 0$ so that S_{free} and S_{rest} are the contributions to the signal at $|\mathbf{q}| = 0$ from the free and restricted compartments, respectively. Dividing both sides of the above equation by $S_{free} + S_{rest}$, we obtain the expression for the NMR signal attenuation for the bi-compartmental system to be

$$E(\mathbf{q}) = f_{free}E_{free}(\mathbf{q}) + f_{rest}E_{rest}(\mathbf{q})$$

where $f_{free} = S_{free}/(S_{free} + S_{rest})$ and $f_{rest} = S_{rest}/(S_{free} + S_{rest})$ satisfy the relationship $f_{free} + f_{rest} = 1$.

Because the spacing between the two NMR tubes is fairly large, diffusion taking place in this region can be assumed to be free. For an arbitrary effective gradient waveform, defined by the function $\mathbf{G}(t)$, applied between the two time points $t = 0$ and $t = T$, the NMR signal attenuation is given by [56]

$$E_{free}(\mathbf{q}) = exp\left[-\gamma^2 D_0 \int_0^T dt \left[\int_0^t \mathbf{G}(t')dt'\right]^2\right],$$

where γ is the gyromagnetic ratio and D_0 is the bulk diffusivity. In this study, four different pulse sequences are employed, one of them is Stejskal and Tanner's standard s-PGSE sequence [9] and the rest are two variants [42] of the d-PGSE sequence [38] as depicted in Fig. 1A and B, and the BPLED sequence [25,55] as shown in Fig. 1C. Evaluating the above expression for the corresponding

effective gradient waveforms, one obtains the free diffusion signal attenuation expressions given by

$$E^{A}_{free}(q) = \exp\left(-8\pi^2 q^2 D_0\left(\Delta - \frac{\delta}{3}\right)\right)$$
$$E^{B}_{free}(q) = \exp\left(-8\pi^2 q^2 D_0\left(\Delta - \frac{\delta}{3} - \frac{\delta}{6}cos(\varphi)\right)\right)$$
$$E^{C}_{free}(q) = \exp\left(-4\pi^2 q^2 D_0\left(\Delta - \frac{\beta}{2} - \frac{\delta}{3}\right)\right)$$

where E^{A}_{free}, E^{B}_{free} and E^{C}_{free} refer to the sequences shown in Fig. 1A ($t_m > \delta$), Fig. 1B ($t_m = 0$) and Fig. 1C, respectively, $q = (2\pi)^{-1}\gamma\delta|\mathbf{G}|$ and φ is the angle between the two gradients employed in the d-PGSE acquisitions. Note that as $\beta \to 0$, $E^{C}_{free}(q)$ tends to the well-known Stejskal–Tanner relationship as expected, which is employed in simulating the signal for free diffusion in s-PFG acquisitions.

In the computations of the signal for restricted diffusion, we employed a generalization [43] of the multiple correlation function (MCF) framework [57]. As shown in [43], the MR signal for a pulse sequence consisting of N gradient pulses, where the n-th pulse of duration δ_n leads to the q-vector $\mathbf{q}_n$, can be written simply to be

$$E_{rest}(q) = \left\langle 0\left|\prod_{n=1}^{N} e^{-\Lambda\delta_n + i2\pi\mathbf{q}_n\cdot\mathbf{A}}\right|0\right\rangle \quad (1)$$

in Dirac's *bra-ket* notation. The infinite-dimensional matrix, Λ, is diagonal. Its elements are given by

$$\langle km|\Lambda|k'm'\rangle = \langle k|k'\rangle\langle m|m\rangle\frac{\alpha^2_{km}D_0}{r_0^2},$$

where r_0 is the radius of the cylinder, and α_{km} is the kth zero of the derivative of the mth-order Bessel function satisfying the expression $J'_m(\alpha_{km}) = 0$. On the other hand, **A** is a vector operator,

$$\mathbf{A} = \begin{pmatrix} X \\ Y \end{pmatrix},$$

where X and Y are infinite-dimensional matrices whose elements are given by

$$\langle km|X|k'm'\rangle = r_0(\langle m|m'+1\rangle + \langle m|m'-1\rangle)(1 + \langle m|0\rangle + \langle m'|0\rangle)^{1/2} \times \beta_{km}\beta_{k'm'}\frac{\alpha^2_{km} + \alpha^2_{k'm} - 2mm}{\left(\alpha^2_{km} - \alpha^2_{k'm'}\right)^2}$$
$$\langle km|Y|k'm'\rangle = ir_0(\langle m|m'+1\rangle -, \langle m|m'-1\rangle)(1 + \langle m|0\rangle + \langle m'|0\rangle)^{1/2} \times \beta_{km}\beta_{k'm'}\frac{\alpha^2_{km} + \alpha^2_{k'm'} - 2mm'}{\left(\alpha^2_{km} - \alpha^2_{k'm'}\right)^2},$$

where

$$\beta_{km} \quad \begin{cases} 1 & \text{if} \quad k = m = 0 \\ \frac{\alpha_{km}}{\left(\alpha^2_{km} - m^2\right)^{1/2}} & \text{otherwise} \end{cases}$$

With these definitions the MR signal for piecewise gradient waveforms can be written down analytically using Eq. (1). The relevant expressions for the pulse sequences of Fig. 1A and B are already provided in [43], hence will not be reproduced here. The corresponding expression for the BPLED sequence is given by

$$E^{C}_{rest}(q) = \langle 0|e^{-\Lambda\delta/2 + i\pi\mathbf{q}\cdot\mathbf{A}}e^{-\Lambda\beta}e^{-\Lambda\delta/2 + i\pi\mathbf{q}\cdot\mathbf{A}}e^{-\Lambda(\Delta-\beta-\delta)}e^{-\Lambda\delta/2 - i\pi\mathbf{q}\cdot\mathbf{A}}e^{-\Lambda\beta}e^{-\Lambda\delta/2 - i\pi\mathbf{q}\cdot\mathbf{A}}|0\rangle^*.$$

In all simulations, Λ, X, and Y matrices of dimension 50×50 were used. Resulting signal attenuation profiles were fitted to experimental data using a Levenberg–Marquardt fitting routine to estimate the cylinder diameter as well as the fractions, f_{free} and f_{rest}.

3. Results

3.1. Relaxation

The free water in the FDC in this experimental setup may have very long T_1 and T_2 relaxation rates. Therefore, to ensure that the signal from the FDC will not be T_1-weighted, we doped it with 1 mM $CuSO_4$. The T_1 of the $CuSO_4$-doped water in the FDC and the water in the microcapillaries in the SDC were found to be 1.50 and 3.10 ± 0.01 seconds respectively. The T_2 of the $CuSO_4$-doped water in the FDC and the water in the microcapillaries in the SDC were found to be 780 and 1280 ± 1 ms.

3.2. Signal decay in the presence of two components

Fig. 2 shows the signal decay for s-PGSE experiments performed on a bi-compartmental phantom consisting of 10 ± 1 μm microcapillaries in the SDC and 20 μl of water in the FDC in both *x*- and *z*- directions. When the diffusion measurement is performed in the *z*-direction, the signal attenuation exhibits a completely free diffusion profile. The diffusion coefficient along the *z*-direction was found to be $D_0 = 1.94 \times 10^{-5}$ cm^2/s.

Inspecting the s-PGSE diffusion measurement in the *x*-direction (black squares) reveals how the fast diffusing component that arises from the FDC affects the signal decay. At relatively low *q*-values, i.e., $q < 450$ cm^{-1}, the attenuation of the signal is completely characteristic of free diffusion, as can be seen by comparison to the *z*-direction data (red circles). At *q* approximately equal to 500 cm^{-1}, a bend in the signal attenuation profile can be seen, above which a restricted profile is observed. Increasing the *q*-value results in diffraction patterns expected from the SDC, with the diffraction trough occurring at $q = 1319$ cm^{-1}, corresponding to a compartment size of 9.24 μm. After the data is fitted to the theory presented above, which corrects for the violation of the SGP approximation, a compartment size of 10.30 ± 0.03 μm is obtained, in good agreement with the nominal ID of 10 ± 1 μm provided by the manufacturer.

3.3. Dependence of the signal decay on the diffusion time

The signal decay for s-PGSE experiments performed on a bi-compartmental phantom consisting of 19 ± 1 μm microcapillaries in the SDC and 80 μl of water in the FDC is shown in Fig. 3 for different values of Δ. Only 6 of the 8 values of Δ measured are shown for clarity. At very short diffusion times, not sufficiently long for a large fraction of water molecules to probe the boundaries of the restricting compartment, the signal decay exhibits a nearly free diffusion profile. When Δ is prolonged, two phenomena can be seen in the different *q*-regimes. For high *q*-values, the diffraction patterns that are expected from water diffusing in the SDC can be gradually observed. At $\Delta = 100$ ms, the diffraction trough is at its deepest, and further prolonging Δ does not change the diffusion profile at high *q*-values, as expected from a restricted diffusion displacement profile. The diffraction troughs occur at $q = 638$ cm^{-1}, corresponding to a size of 19.12 μm, which is consistent with the nominal ID of the microcapillaries, 19 ± 1 μm. However, at lower *q*-values, e.g., $q < 200$ cm^{-1}, the diffusion curve changes dramatically for each value of Δ, and shows increased attenuation of the signal for every value of increasing Δ (Fig. 3). The theoretical curves fit all of the experimental data nicely.

The results of the fittings of the signal decay from this experiment to the theory presented above are summarized in Table 1. Already at $\Delta = 25$ ms, a size of 19.31 ± 0.09 μm is extracted, which represents the accurate nominal size of the SDC. Similar characteristic compartment dimensions are extracted for longer Δs. Note

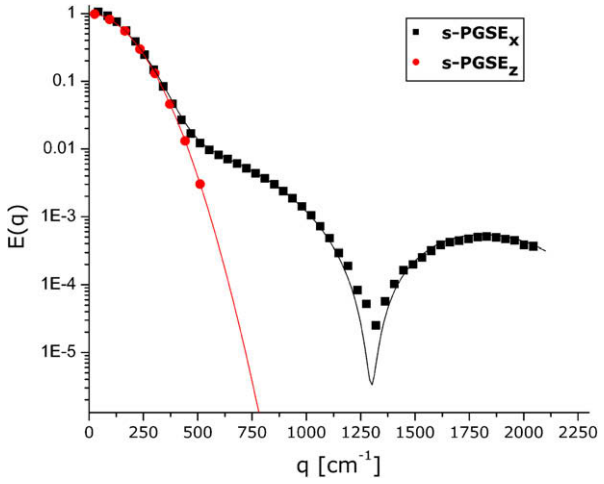

Fig. 2. s-PGSE experiments in the presence of the fast and slow components: *x*- and *z*-directions. The bi-compartmental phantom consisted of microcapillaries with ID of 10 ± 1 μm as the SDC and 20 μl of water in the FDC. The s-PGSE was conducted with Δ/δ of 30/3 ms. The black squares represent the measurement in the *x*-direction, and the red circles represent the *z*-direction measurement. Symbols indicate experimental data and the solid lines represent the theoretical curves. (For interpretation of color mentioned in this figure legend the reader is referred to the web version of the article.)

that at Δ = 25 ms, an accurate size cannot be extracted from the diffraction patterns, because the diffractions are too shallow.

3.4. Dependence of the signal decay on the amount of water in the FDC

To investigate how the signal decay is affected by increasing the relative fraction of the fast diffusing component, 19 ± 1 μm microcapillaries were first measured without an FDC. Subsequently, increasing amounts of water were added to the FDC. Fig. 4 shows the results. When water is not present in the FDC, the signal exhibits the attenuation that is characteristic of restricted diffusion, with the diffraction trough at q = 638 cm^{-1}, in agreement with the nominal ID of 19 ± 1 μm (black squares). Here, at $q \sim 250$ cm^{-1}, E(q) is equal to 0.54. However, when 20 or 100 μl of water are added to the FDC (red circles and green triangles, respectively), the bend

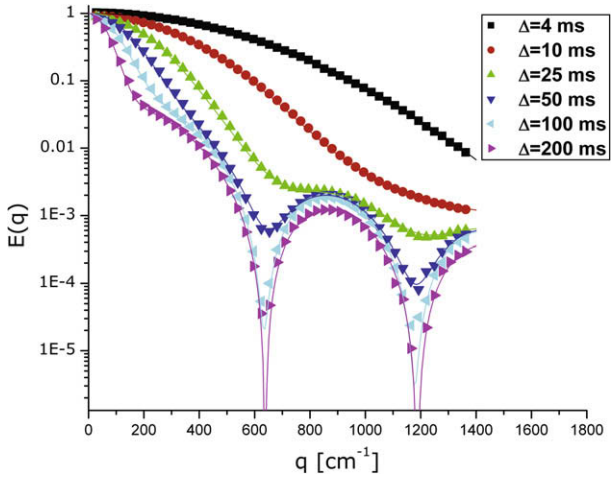

Fig. 3. Dependence of the signal decay on the diffusion time in s-PGSE experiments. The bi-compartmental phantom was used with 19 ± 1 μm microcapillaries as the SDC and 80 μl of water in the FDC. $E(q)$ data from s-PGSE experiments conducted in the *x*-direction are plotted against q for different values of Δ. Symbols represent experimental data while solid lines represent the theoretical curves for these data.

Table 1
Extracted size as a function of Δ in s-PGSE experiments, performed on a bi-compartmental phantom with 80 μl of water in the FDC and 19 ± 1 microcapillaries in the SDC.

Diffusion time (Δ) (ms)	ID (μm)
4	6.71 ± 0.01
10	47.22 ± 1.44
25	19.31 ± 0.09
50	19.42 ± 0.02
75	19.42 ± 0.02
100	19.43 ± 0.02
150	19.44 ± 0.02
200	19.30 ± 0.02

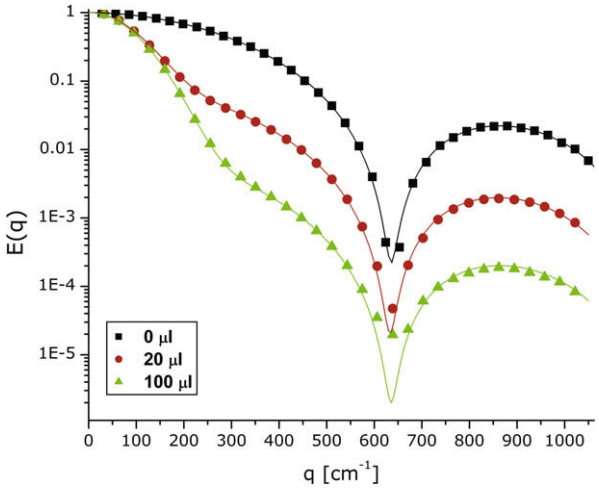

Fig. 4. Dependence of the signal decay on the amount of water in the FDC in s-PGSE experiments. The bi-compartmental phantom consisted of microcapillaries with ID of 19 ± 1 μm as the SDC. The black squares represent the separate microcapillaries sample. The red circles and green triangles represent 20 and 100 μl of water in the FDC, respectively. The s-PGSE measurement was conducted in the *x*-direction with Δ/δ = 100/2 ms. Symbols indicate experimental data and the solid lines represent the theoretical curves. (For interpretation of color mentioned in this figure legend the reader is referred to the web version of the article.)

in the signal decay which indicates the transition between free and restricted diffusion can be seen at around $q \sim 250$ and 290 cm^{-1}, respectively. Note that below the q-value at which the transition between free and restricted diffusion occurs, the signal attenuation is stronger with increasing volume fraction of FDC. For example for 20 and 100 μl of water in the FDC, the signal attenuates to 0.055 and 0.013 respectively at q = 255 cm^{-1}. The solid curves, representing the theoretical fitting of the data, are in very good agreement with the experimental data. The sizes that were extracted for the microcapillaries, as summarized in Table 2, are in good agreement with the nominal ID provided by the manufacturer. Note the increase in the fraction of free water with increasing amount of water, and that for the sample consisting of no water in the FDC, the extracted fraction of water is close to 0. Similar

Table 2
Sizes and fractions of restricted and free water components as a function of amount of water in the FDC extracted from the s-PGSE experiments.

Amount of water in the FDC[a]	0 μl	20 μl	100 μl
ID (μm)	19.39 ± 0.02	19.46 ± 0.03	19.39 ± 0.08
f_{rest}	0.980 ± 0.002	0.087 ± 0.002	0.0088 ± 0.0004
f_{free}	0.021 ± 0.002	0.91 ± 0.05	0.99 ± 0.08

[a] A bi-compartmental phantom with 19 ± 1 microcapillaries in the SDC was used. The diffusion time in this experiment was Δ = 100 ms.

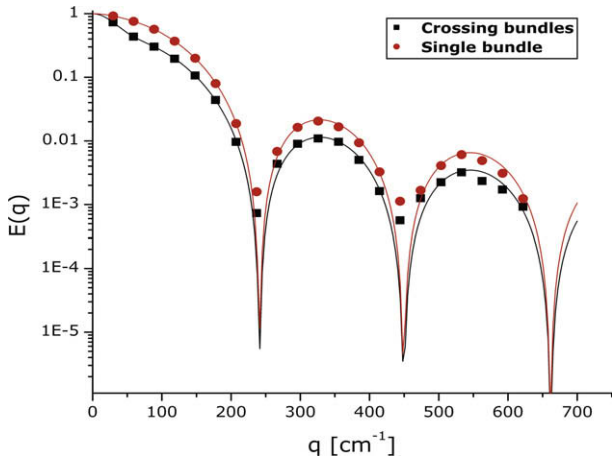

Fig. 5. Signal decay in the crossing fibers phantom obtained from the BPLED experiments. Microcapillaries with ID of 48 ± 1 μm were used as described in Section 2 and Fig. 1E and F. The BPLED sequence was used to overcome the inhomogeneity of the sample with Δ/δ = 1000/10 ms. The black squares represent the data from crossing fibers, while the red circles represent the data from a single bundle. The solid lines represent the theoretical curves fitted to the data. (For interpretation of color mentioned in this figure legend the reader is referred to the web version of the article.)

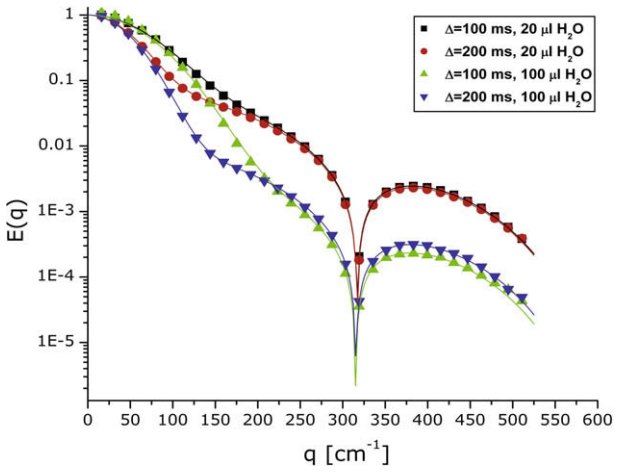

Fig. 6. The signal decay in d-PGSE experiments conducted on the bi-compartmental phantom. Microcapillaries with ID = 19 ± 1 μm were used as the SDC. The black squares and upward green triangles represent the experimental data for the d-PGSE measurements in which $\Delta_1 = \Delta_2$ = 100 ms and the amount of FDC was 20 μl. The red circles and downward blue triangles represent the experimental data for the d-PGSE measurements in which $\Delta_1 = \Delta_2$ = 200 ms and the amount of FDC was 100 μl. The solid lines represent the theoretical curves fitted to the data. (For interpretation of color mentioned in this figure legend the reader is referred to the web version of the article.)

results were obtained for s-PGSE experiments conducted on the same phantom with Δ = 200 ms (data not shown).

3.5. Crossing fibers phantom

Fig. 5 shows the signal decay from a phantom consisting of bundles of crossing fibers with IDs of 48 ± 1 μm and from one fiber bundle of 48 ± 1 μm microcapillaries for comparison. Note that the bi-polar LED sequence was used here to overcome the severe susceptibility artifact that arises in such phantoms [25].

The single fiber bundle exhibits the signal decay expected from the restricted compartment in the fibers, with the first diffraction trough occurring at q = 237 cm^{-1} (red circles). However, when the second bundle of fibers is added, the contribution of the fast diffusing component that comes from diffusion along the main axis of the fiber becomes apparent (black squares). The comparison reveals that the attenuation of the signal resembles that of the bi-compartmental phantom. At the first low q-values, where the free diffusion behavior dominates, a stronger attenuation of the signal is apparent when compared to the single bundle at low q-values. The first diffraction trough occurs at q = 237 cm^{-1}, corresponding to a size of 51.5 μm, which is within a 6% of the nominal ID of 48 ± 1 μm. The theoretical curves are in good agreement with the experimental data, and the compartment dimensions and volume fractions are summarized in Table 3. Note that for the crossing fibers, the volume fractions of free and restricted compartments have a ~1:1 ratio, consistent with the fact that a very similar number of fibers were present in each bundle.

Table 3
Sizes and fractions of restricted and free water in the crossing fibers phantom, extracted from the BP-LED experiments.

	Crossing fibers[a]	Single fiber bundle[a]
ID (μm)	51.10 ± 0.07	51.14 ± 0.06
f_{rest}	0.499 ± 0.001	0.939 ± 0.001
f_{free}	0.501 ± 0.002	0.061 ± 0.004

[a] The nominal ID of the microcapillaries used in this phantom was 48 ± 1 μm. The BPLED sequence was used to overcome the inhomogeneity induced by the crossing fibers with Δ/δ = 1000/10 ms.

3.6. High q d-PGSE experiments on the bi-compartmental model

Similar to the experiments performed using the s-PGSE, we tested the dependence of the signal decay in d-PGSE on the diffusion times and amount of water present in the FDC. For these experiments, the SDC consisted of 19 ± 1 μm microcapillaries. The results from the d-PGSE experiment for two different amounts of water (20 and 100 μl) in the FDC and for two diffusion times, i.e., $\Delta_1 = \Delta_2$ = 100 or 200 ms, are shown in Fig. 6. For all of these experiments the diffraction trough occurs at half of the q-value of the s-PGSE, namely q = 317 cm^{-1}, as expected. The results presented in Fig. 6 are magnitude calculated; however, it is important to note that the diffractions exhibited the zero crossing of the signal, characteristic to d-PGSE diffractions (negative diffractions) [50,51]. Fig. 6 demonstrates that the signal decay in d-PGSE experiments resembles all of the signal trends that were shown for s-PGSE. The two diffusion modes can be easily observed, and the characteristic bend in the signal decay which indicates the transition between free and restricted diffusion profiles, can be seen, e.g., at q = 126 cm^{-1} for $\Delta_1 = \Delta_2$ = 200 ms and 100 μl of water in the FDC. For both amounts of water in the FDC, increasing the diffusion times from 100 to 200 ms results in a reduction of the q-value at which the transition from the free profile to the restricted profile occurs. Additionally, for each diffusion time, when the volume of water in the FDC is increased from 20 μl to 100 μl, the q value at which the transition between the free and restricted diffusion profiles shifts to higher q-values. The theoretical curves are in good agreement with experimental data, and the fitting results are summarized in Table 4. For all measurements, the compartment size that is extracted is in very good agreement with the nominal ID of 19 ± 1 μm.

3.7. Comparing d-PGSE and s-PGSE experiments

When only one restricted compartment exists, scaling the q-axis by a factor of two for the d-PFG data yields a similar attenuation profile, as compared to the matched s-PGF experiment. Under these conditions, the first zero crossing occurs at the same point where the s-PFG trough is observed [50,51]. However, this is not

Table 4
Sizes and fractions of restricted water components in the bi-compartmental phantom extracted from d-PGSE experiments.

	20 μl $\Delta_1 = \Delta_2 = 100$ ms	100 μl $\Delta_1 = \Delta_2 = 100$ ms	20 μl $\Delta_1 = \Delta_2 = 200$ ms	100 μl $\Delta_1 = \Delta_2 = 200$ ms
ID (μm)[a]	19.451 ± 0.004	19.55 ± 0.02	19.417 ± 0.004	19.51 ± 0.01
f_{rest}	0.087 ± 0.0005	0.0083 ± 0.0002	0.0815 ± 0.0005	0.011 ± 0.0009

[a] The nominal ID of the microcapillaries used in the SDC in this phantom was 19 ± 1 μm. The d-PGSE sequence was performed with $\varphi = 0$, i.e. both $\mathbf{G}_1$ and $\mathbf{G}_2$ were in the x-direction, and $\delta_1 = \delta_2 = \delta_3 = 2$ ms.

the case in a bi-compartmental model. To be able to compare the signal decay of s- and d-PGSE experiments, a bi-compartmental phantom with 19 ± 1 μm microcapillaries as the SDC and 100 μl of water in the FDC was used. Fig. 7A and B shows the signal decay from a s-PGSE experiment plotted against q (black squares) while the d-PGSE experiments are plotted against $2q$ or $2^{1/2}q$ (red circles), respectively. The s-PGSE, serving here as a control experiment, reveals the signal decay characteristic of the bi-compartmental model, with a diffraction trough at $q = 638$ cm^{-1} (Fig. 7A and B). However, it is impossible to scale the d-PGSE experiment such that the signal attenuation will match that of the s-PGSE. It is apparent that when the two diffusing components coexist, the signal decay cannot be directly compared in the high- and low-q regimes. The diffraction troughs occur at the expected q for d-PGSE experiments when the data is plotted against $2q$; however, using the $2q$ scaling appears to stretch the regime in which the free diffusion from the FDC dominates. Scaling the plot of the d-PGSE data against $2^{1/2}q$ reveals that the signal from the FDC can be directly compared, but the diffraction troughs of the d-PGSE experiment occur at a different location on the horizontal axis for this scaling. Similar results were obtained for microcapillaries with ID of 10 ± 1 μm, for different values of Δs, and for varying amounts of freely diffusing water in the FDC (data not shown). Note that the theoretical curves are in good agreement with the experimental results.

3.8. Angular d-PGSE experiments in the bi-compartmental phantom

Previously, we demonstrated the ability of the angular d-PGSE experiment to reveal microscopic anisotropy even at low q-values in a single restricted compartment [43,44], from which the accurate dimension of the compartment could be extracted. However the signal decay in the bi-compartmental phantoms is masked by the freely diffusing component at low q-values and the restriction in the SDC is only revealed at higher q-values, as was shown in Figs. 3 and 4. To test how microscopic anisotropy is affected by the freely diffusing component, we used 19 ± 1 μm microcapillaries as the SDC and 20 μl of water in the FDC to perform the angular d-PGSE experiment at various q-values and with diffusion times $\Delta_1 = \Delta_2 = 100$ or 200 ms. Fig. 8A shows the signal decay from the d-PGSE experiment for $\varphi = 0°$ up to $q = 300$ cm^{-1} for the two diffusion times. As demonstrated above, for $\Delta_1 = \Delta_2 = 200$ ms, the signal decays more significantly when compared to $\Delta_1 = \Delta_2 = 100$ ms in the low-q regime. Since both diffusion times are long enough to completely probe the boundaries, the NMR signals for both diffusion times decay towards a diffraction trough at $q = 319$ cm^{-1} (note that the data are magnitude calculated, for clarity, and therefore the signal decay approaches a diffraction trough instead of a zero crossing). Fig. 8B and C demonstrates the angular experiment for which the diffusion times were set to $\Delta_1 = \Delta_2 = 100$ ms for the q-values highlighted by vertical lines in Fig. 8A (only 9 of the 16 q-values collected are shown). Fig. 8B shows the angular dependence at q-values in which the free diffusion profile is prominent (as shown in Fig. 8A), while Fig. 8C shows the angular dependence at higher q-values, in which the restricted diffusion begins to take over. At the regime in which free diffusion is more prominent, i.e., for $q < 100$ cm^{-1}, the signal decay exhibits no angular dependence, and only sporadic signal fluctuations are observed. The theoretical curves are in good agreement with the experimental data. At higher q-values however, approximately $q \sim 125$ cm^{-1} and higher, the angular dependence of the signal decay becomes more pronounced and the bell-shaped function becomes gradually more apparent. The stack plot of the signal as a function of φ values at $q = 53$, 129 and 298 cm^{-1} is shown in Fig. 8D. From this figure, which rep-

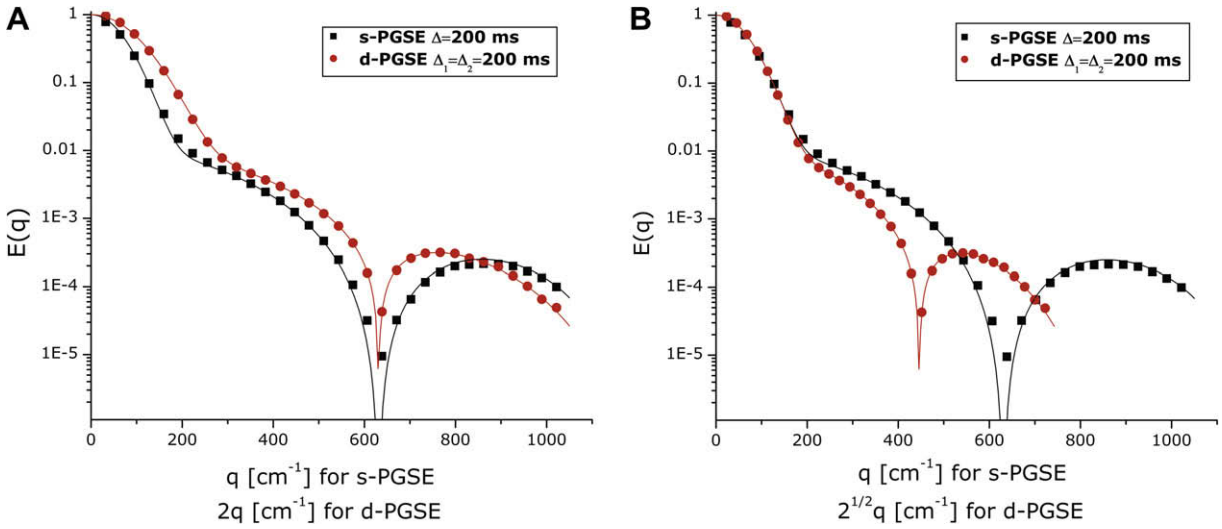

Fig. 7. Comparison between s-PGSE and d-PGSE measurements. The bi-compartmental phantom consisted of microcapillaries with ID = 19 ± 1 μm as the SDC and 100 μl of water in the FDC. (A) The s-PGSE data is plotted against q (black squares) while the d-PGSE is plotted against $2q$ (red circles). (B) The s-PGSE data is plotted against q (black squares) while the d-PGSE data is plotted against $2^{1/2}q$ (red circles). The solid lines represent the theoretical curves fitted to the data. (For interpretation of color mentioned in this figure legend the reader is referred to the web version of the article.)

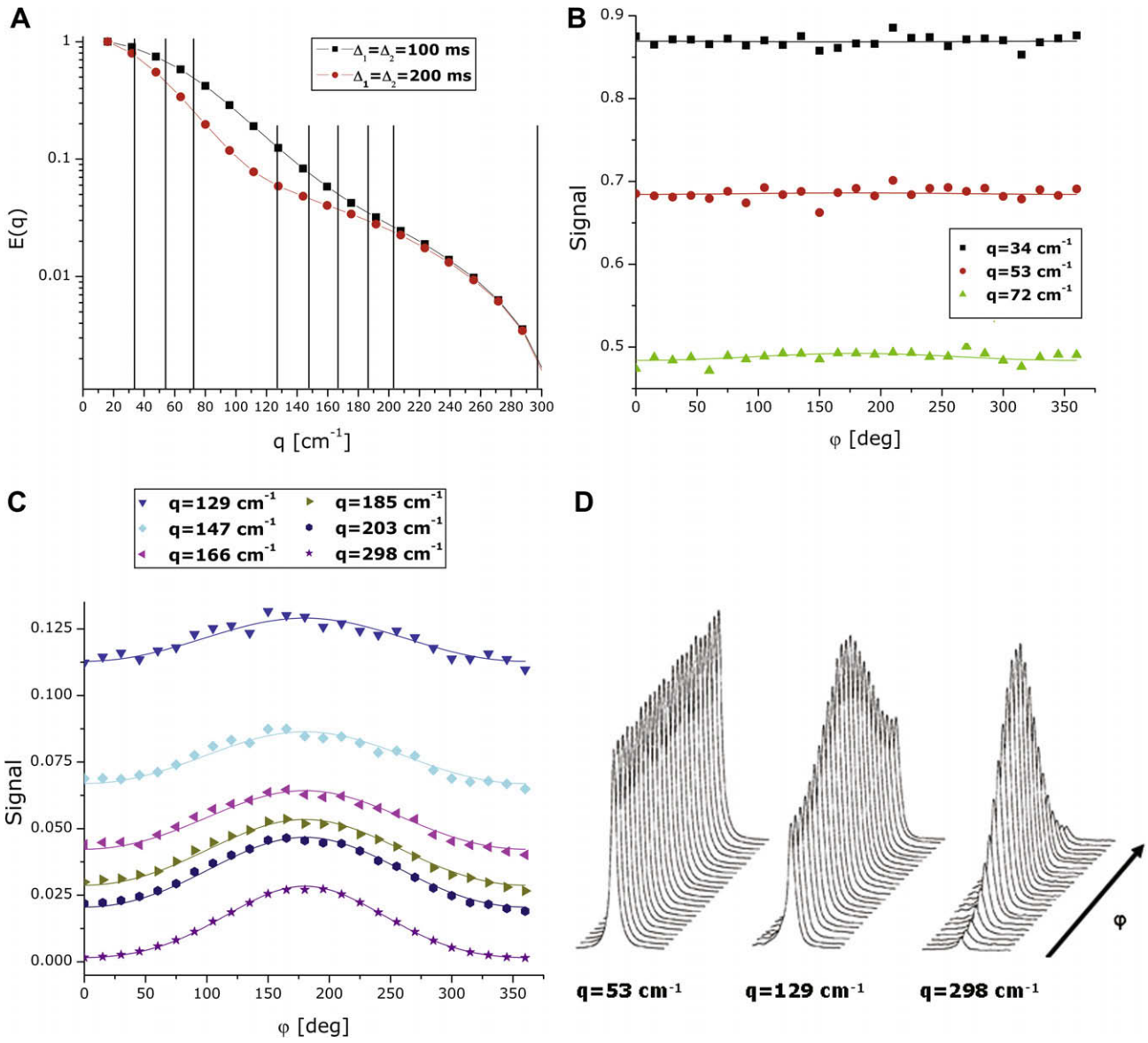

Fig. 8. Angular d-PGSE experiments. The bi-compartmental phantom consisted of microcapillaries with ID = 19 ± 1 μm as the SDC and 20 μl of water in the FDC. (A) The d-PGSE data for $\varphi = 0°$. The diffusion times in these experiments were $\Delta_1 = \Delta_2 = 100$ or 200 ms (black squares and red circles, respectively). The vertical black lines represent the q-values for which the angular profile is presented in (B) and (C). (B) The signal intensity plotted against φ for the q-values between 34 and 72 cm^{-1}. (C) The signal intensity plotted against φ for the q-values between 129 and 298 cm^{-1}. The solid curves in (A)–(C) represent the theoretical fitting of the experimental data. (D) Raw data for 3 selected q-values of the signal intensity plotted against φ. (For interpretation of color mentioned in this figure legend the reader is referred to the web version of the article.)

resents the raw data from this experiment, it is clear that the signal at low q-values does not have a clear angular dependence but suffers from random fluctuations, while the bell-shaped function becomes more pronounced at higher q-values. The theoretical curves again fit nicely through the experimental points. Table 5 summarizes the sizes that are extracted for the angular experiments for several values of q for both diffusion times, i.e. $\Delta_1 = \Delta_2 = 100$ and 200 ms. Note that for both diffusion times, the higher the q value, the lower the error in the compartment size extracted. Moreover, for $\Delta_1 = \Delta_2 = 100$ and 200 ms, the q-values at which a very accurate estimate of the dimension of the microcapillaries is extracted are 185 and 166 cm^{-1}, respectively, indicating that when a longer Δ is applied, microscopic anisotropy can be restored at lower q-values.

Table 5
Extracted sizes for several q-values from the angular d-PGSE experiment.

q Value[a]	34 cm^{-1}	72 cm^{-1}	109 cm^{-1}	129 cm^{-1}	166 cm^{-1}	185 cm^{-1}	298 cm^{-1}
ID (μm) ($\Delta_1 = \Delta_2 = 100$ ms)	1 ± 865	26 ± 4	23.5 ± 1.2	21.75 ± 0.75	20.3 ± 0.3	19.90 ± 0.25	19.44 ± 0.03
ID (μm) ($\Delta_1 = \Delta_2 = 200$ ms)	33 ± 2	30 ± 1	21.7 ± 0.7	20.0 ± 0.5	19.7 ± 0.3	19.61 ± 0.22	19.42 ± 0.02

[a] The angular d-PGSE experiment was performed on the bi-compartmental phantom with 20 μl of water in the FDC and 19 ± 1 μm microcapillaries in the SDC. For this set of experiments $\delta_1 = \delta_2 = \delta_3 = 2$ ms.

4. Discussion

Instances for which at least two diffusion modes co-exist may appear in a variety of systems, including porous materials and biological tissues. In this study, we have used a simplified bi-compartmental model, which consists of two well-defined compartments: the fast diffusion compartment, which has the diffusivity of free water, and the slow diffusion compartment, which has the diffusion characteristics of the restricted compartment. Using such a simplified phantom is suitable for testing the theory presented above, and to understand how the different diffusion modes contribute to the signal decay.

When diffusion is measured along the z-direction, i.e. parallel to the main axis of the microcapillaries, free diffusion dominates. However, when diffusion is measured along the x-axis, perpendicular to the main axis of the fibers, the different diffusion modes are accentuated at different q-regimes. At the low-q regime, the signal is governed by free diffusion, and the restricted compartment is masked. However, when higher q-values are reached, the signal decay demonstrates a characteristic bending, which indicates the "taking over" of the restricted diffusion mode. The bend in the signal decay was observed at different q-values for different microcapillaries, and is apparently a function of the amount of water present in FDC and the diffusion time. Notably, at even higher q-values, the structural features present in the sample could still be resolved by both the diffraction patterns and the fitted theoretical curves, even when the amount of water in the FDC was very large, providing that the diffusion time was sufficiently long to probe the boundaries of the restricted compartment.

The dependence of the signal decay in s-PGSE experiments on Δ and on the amount of water in the FDC was also tested. We found that for very short Δs, a nearly free diffusion profile is obtained even at high values of q, and that when prolonging the Δ the restriction is gradually sampled, as implied by the steady appearance of the diffraction troughs and the extraction of the correct compartment sizes by the theory. This implies that in order to extract meaningful structural information, the point of maximum restriction must be reached. It has been previously shown that for a single restricted compartment, prolonging Δ after the point in which maximum restriction is sampled does not lead to any further changes in the diffusion profile [15], a fact that can be used to determine the minimum value of Δ for fully sampling restriction. Indeed, even when the fast component is introduced, prolonging Δ does not affect the signal decay at the q-values in which restricted diffusion is apparent. However, at low q-values, the fast diffusing component exhibits continuous attenuation of the signal when Δ is prolonged: the longer the Δ, the lower the q value in which the restricted diffusion becomes apparent.

When the amount of water in the FDC is increased from 20 to 100 μl, the q-values at which the bend in the signal decay which indicates the transition from free to restricted diffusion profiles shifts from $q \sim 250\ \mathrm{cm}^{-1}$ to $q \sim 290\ \mathrm{cm}^{-1}$ as shown in Fig. 4. This shift to higher q-values was also observed in bi-compartmental models with smaller sizes of microcapillaries in the SDC (data not shown). Our simulations suggest that a smoothing effect of the diffraction troughs and even a shift in their location to higher q-values may occur solely due to the presence of a fast diffusing component (data not shown). This effect is particularly important at relatively short diffusion times, or more generally, if there is significant signal due to free diffusion around the q-values at which the trough due to the SDC is expected.

Our findings suggest that when the slow diffusing component is of interest, usually for purposes of extraction of structural information, high q-values are preferable, especially if the fraction of the fast diffusing component is large. Even when the fraction ratios are ~1, a more realistic setting for biological tissues, higher q-values are preferable for extracting structural information. This is demonstrated by the crossing fibers phantom, for which the fractions of FDC and SDC are very similar. The first diffraction trough already occurs at a relatively low q-value because of the large ID of the fibers that were used in this study. Nevertheless, the signal decay at lower q-values exhibits a free diffusion profile. Since the diffusion time used was extremely long (Δ = 1000 ms), the transition from the free diffusion profile to the restricted diffusion profile occurred at a very low-q of $\sim 60\ \mathrm{cm}^{-1}$. Crossing fibers are generally problematic to resolve by DTI, because the gradients that are applied perpendicular to the main axis of one bundle are also parallel to the main axis of the second bundle, creating a bi-compartmental system. The data observed in our composite bi-compartmental phantom, as well as the crossing fibers phantom suggest that at low q-values which are customary for DTI measurements, the fast diffusing component will be prominent, and will mask the restricted diffusion occurring in the perpendicular fiber, yielding a reduction in the observed anisotropy. However, it seems that by prolonging Δ, one may eliminate the fast diffusing component even at low-q, and sample anisotropy even in crossing fibers. Another option to accentuate the restricted compartment is to simply measure the signal decay at higher q-values. In the present study, the microcapillaries in crossing fibers phantom were perpendicular to each other; therefore a free diffusion profile was observed in the low q-regime in addition to the restricted profile observed in higher q-values. However, in more realistic cases, when the angle between the microcapillaries is not 90° but more acute, a diffusion measurement perpendicular to one of the main axis of the microcapillaries would yield a smaller fast component at the low q-regime. Nevertheless, at higher q-values, the diffusion–diffraction pattern from the restricted diffusion would still persist, and the compartment size could be extracted.

The same trends that were observed in the signal decay for s-PGSE due to changes in diffusion times and amounts of water in the FDC apply for d-PGSE experiments, but a direct comparison between the s-PGSE and the d-PGSE is impossible to perform. When only one diffusing component exists in a restricted compartment, the comparison can be made by scaling the d-PGSE q axis by a factor of 2, as demonstrated in [51]. When only a single free diffusion compartment is present, the comparison can be made by scaling the d-PGSE q-axis by a factor of $2^{1/2}$ (unpublished results). When trying to compare the s-PGSE and d-PGSE data in the bi-compartmental phantom, where both diffusion modes co-exist, scaling the q axis by 2 and $2^{1/2}$ enabled direct comparison of the restricted and free q regimes, respectively, but incurred incomparability for the reciprocal diffusion mode. These findings may be of importance in investigations on biological tissues or porous media, where a comparison between the two methodologies may be beneficial, especially since the d-PFG experiment may be more robust towards size distributions [50,51].

The angular d-PGSE experiment has been used recently to measure small compartmental dimensions at low q-values [43,44], a methodology that obviates very powerful gradients used for characterizing restricted compartments using s-PGSE. The angular dependence of the signal decay originates from the microscopic anisotropy induced by the boundaries of the confining compartment, providing that the diffusion times are long enough to probe the boundaries of the restricting compartment. In the bi-compartmental model, however, we demonstrated that at q-values in which the free diffusion profile is prominent, there is no detectable angular dependence in the signal decay. This observation implies that free diffusion, arising from the free water in the FDC, is masking the signal arising from the restricted compartment almost completely, and that the anisotropy induced by the boundaries of

the restricting compartment is suppressed for these q-values. We have demonstrated that prolonging the diffusion times shifts the q of transition between free and restricted diffusion profiles to lower q-values; this applies also for the angular dependence, which can be seen for lower q-values if the diffusion times are prolonged (Table 5 and Fig. 8). This may be of importance especially in biological tissues, because it means that by increasing the diffusion times one may sample microscopic anisotropy from different compartments at the same q-value. Though not demonstrated here, these findings are expected to be valid in the extraction of compartment shape anisotropy (CSA) using angular double-PFG experiments, as studied recently in [58].

The angular d-PGSE experiments in this model also reveal that the higher the q-value, the lower the error in the estimated compartment size. This is probably due to the complete suppression of the fast diffusing component at higher q-values. However, the estimates for the compartment dimension from the angular d-PGSE experiment were largely affected when even slight changes were made to the water bulk diffusivity parameter (D_0) in the fits. This implies that an accurate measurement of D_0 is crucial for the correct estimate of compartment size. It is interesting to note that this is not the case for the more conventional d-PGSE datasets (i.e. $E(\mathbf{q})$ for $\varphi = 0^\circ$), where slight variations in the D_0 parameter did not alter the results significantly (data not shown).

It is noteworthy that realistic systems are often heterogeneous and are characterized by size distributions. This has been shown to significantly limit the structural information that can be obtained from s-PFG experiments [50,59]. Previously, we have shown that the d-PFG experiment is more robust towards size distribution theoretically [50] and, experimentally [51]. The experiments in the present study were performed on a homogenous sample which has a negligible size distribution, and therefore both s-PFG and d-PFG experiments revealed diffusion–diffraction troughs; in samples which contain both size distributions and unrestricted compartments, the d-PFG may have an advantage over the s-PFG.

A few recent studies have employed different variants of the d-PFG acquisitions in studies of phantoms and even biological tissue [60–62]. In fact in Ref. [61], the authors have expressed the MR signal as the sum of two terms: the slow diffusing component, arising from an SDC employed Mitra's original expression, whereas the diffusion signal arising from the FDC has been approximated by an expansion of the Gaussian decay up to the quadratic term. However, Mitra's theory [52] applies only in limiting cases that cannot be reached experimentally. In fact, in [44], we have shown that even when only a single component exists, the experimental parameters have a profound effect on the size extracted using Mitra's theory. Moreover, expressing the FDC term as a quadratic polynomial further narrows the regime in which the technique will be applicable as even modest b-values around 1000 s/mm^2 leads to significant deviations from the correct form of the signal attenuation. As demonstrated, the theory employed in our work is valid and leads to accurate estimations for a much wider range of experimental parameters. Moreover, our current work shows that at different q-values, different components are emphasized in the angular dependence of the signal decay. As a result, the signal from a free diffusion compartment may dominate the low-q regime—the same regime in which Mitra's theory is valid. Thus it may be necessary to employ a more general theory, such as that employed in this study, to infer the compartment size when a free diffusion compartment co-exists with the slow diffusion compartment.

5. Conclusions

Diffusion measurements performed on bi-compartmental phantoms provide insight on how the signal decay in restricted compartments is affected by the presence of a free diffusion compartment. At low q-values, the restricted diffusion behavior is masked by the fast diffusing component; a free diffusion profile is obtained, and no anisotropy is detected. We found that the q-value at which the transition from a free diffusion profile to a restricted diffusion profile occurs depends on the diffusion times and on the fraction of the fast diffusing component. The theory presented here corroborates the experimental results, and allows quantification of the fraction of free and restricted compartments, as well as the compartment dimensions and the rmsd of the free diffusing component. We have also demonstrated the usefulness of this model in describing NMR signal decay in a crossing fiber phantom. The d-PGSE data show the same trends as the s-PGSE, but a direct comparison between the two methodologies is not straightforward due to the different scaling laws required in each diffusion regime. The angular d-PGSE experiment is useful in quantifying the microscopic anisotropy induced by the boundaries of the restricting compartment, and the absence of microscopic anisotropy at low q-values suggests that free diffusion may mask the features of restricted diffusion in that regime. This study may be useful for further quantifying restricted diffusion in more realistic model systems such as biological tissues and porous materials.

Acknowledgments

P.J.B and E.Ö. were supported by the Intramural Research Program of the Eunice Kennedy Shriver National Institute of Child Health and Human Development.

References

[1] Y. Cohen, Y. Assaf, High b-value q-space analyzed diffusion-weighted MRS and MRI in neuronal tissues—a technical review, NMR Biomed. 15 (2002) 516–542.
[2] Y. Cohen, L. Avram, L. Frish, Diffusion NMR spectroscopy in supramolecular and combinatorial chemistry: an old parameter—New insights, Angew. Chem. Int. Ed. 44 (2005) 520–554.
[3] A. Dehner, H. Kessler, Diffusion NMR spectroscopy: folding and aggregation of domains in p53, Chembiochem 6 (2005) 1550–1565.
[4] D. LeBihan, Molecular diffusion, tissue microdynamics and microstructure, NMR Biomed. 8 (1995) 375–386.
[5] L.H. Lucas, C.K. Larive, Measuring ligand–protein binding using NMR diffusion experiments, Concepts Magn. Reson. A 20A (2004) 24–41.
[6] M. Stjerndahl, D. Lundberg, H.L. Zhang, F.M. Menger, NMR studies of aggregation and hydration of surfactants containing amide bonds, J. Phys. Chem. B 111 (2007) 2008–2014.
[7] P.N. Sen, Diffusion and tissue microstructure, J. Phys. Condens. Matter. 16 (2004) S5213–S5220.
[8] P.N. Sen, Time-dependent diffusion coefficient as a probe of geometry, Concepts Magn. Reson. A 23A (2004) 1–21.
[9] E.O. Stejskal, J.E. Tanner, Spin diffusion measurements—spin echoes in presence of a time-dependent field gradient, J. Chem. Phys. 42 (1965) 288–292.
[10] J.E. Tanner, Use of stimulated echo in NMR-diffusion studies, J. Chem. Phys. 52 (1970) 2523–2526.
[11] W.S. Price, Pulsed-field gradient nuclear magnetic resonance as a tool for studying translational diffusion. 1. Basic theory, Concepts Magn. Reson. 9 (1997) 299–336.
[12] P.T. Callaghan, A. Coy, D. Macgowan, K.J. Packer, F.O. Zelaya, Diffraction-like effects in NMR diffusion studies of fluids in porous solids, Nature 351 (1991) 467–469.
[13] P.T. Callaghan, NMR imaging, NMR diffraction and applications of pulsed gradient spin echoes in porous media, Magn. Reson. Imaging 14 (1996) 701–709.
[14] L. Avram, Y. Assaf, Y. Cohen, The effect of rotational angle and experimental parameters on the diffraction patterns and micro-structural information obtained from q-space diffusion NMR: implication for diffusion in white matter fibers, J. Magn. Reson. 169 (2004) 30–38.
[15] L. Avram, E. Özarslan, Y. Assaf, A. Bar-Shir, Y. Cohen, P.J. Basser, Three-dimensional water diffusion in impermeable cylindrical tubes: theory versus experiments, NMR Biomed. 21 (2008) 888–898.
[16] A. Bar-Shir, Y. Cohen, The effect of the rotational angle on MR diffusion indices in nerves: is the rms displacement of the slow-diffusing component a good measure of fiber orientation?, J Magn. Reson. 190 (2008) 33–42.
[17] A. Bar-Shir, L. Avram, E. Ozarslan, P.J. Basser, Y. Cohen, The effect of the diffusion time and pulse gradient duration ratio on the diffraction pattern and

the structural information estimated from q-space diffusion MR: experiments and simulations, J. Magn. Reson. 194 (2008) 230–236.
[18] P.T. Callaghan, Pulsed-gradient spin-echo NMR for planar, cylindrical, and spherical pores under conditions of wall relaxation, J. Magn. Reson. A 113 (1995) 53–59.
[19] S.L. Codd, P.T. Callaghan, Spin echo analysis of restricted diffusion under generalized gradient waveforms: planar, cylindrical, and spherical pores with wall relaxivity, J. Magn. Reson. 137 (1999) 358–372.
[20] A.V. Barzykin, Theory of spin echo in restricted geometries under a step-wise gradient pulse sequence, J. Magn. Reson. 139 (1999) 342–353.
[21] B.N. Ryland, P.T. Callaghan, Spin echo analysis of restricted diffusion under generalized gradient waveforms for spherical pores with relaxivity and interconnections, Isr. J. Chem. 43 (2003) 1–7.
[22] P.W. Kuchel, A. Coy, P. Stilbs, NMR "diffusion–diffraction" of water revealing alignment of erythrocytes in a magnetic field and their dimensions and membrane transport characteristics, Magn. Reson. Med. 37 (1997) 637–643.
[23] J.F. Kuntz, P. Palmas, D. Canet, Diffusive diffraction measurements in porous media: effect of structural disorder and internal magnetic field gradients, J. Magn. Reson. 188 (2007) 322–329.
[24] J.F. Kuntz, G. Trausch, P. Palmas, P. Mutzenhardt, D. Canet, Diffusive diffraction phenomenon in a porous polymer material observed by NMR using radio-frequency field gradients, J. Chem. Phys. 126 (2007) 134904.
[25] A. Bar-Shir, Y. Cohen, Crossing fibers, diffractions and nonhomogeneous magnetic field: correction of artifacts by bipolar gradient pulses, Magn. Reson. Imaging 26 (2008) 801–808.
[26] D.G. Cory, A.N. Garroway, Measurement of translational displacement probabilities by NMR—an indicator of compartmentation, Magn. Reson. Med. 14 (1990) 435–444.
[27] P.W. Kuchel, T.R. Eykyn, D.G. Regan, Measurement of compartment size in q-space experiments: Fourier transform of the second derivative, Magn. Reson. Med. 52 (2004) 907–912.
[28] Y. Assaf, Y. Cohen, Non-mono-exponential attenuation of water and N-acetyl aspartate signals due to diffusion in brain tissue, J. Magn. Reson. 131 (1998) 69–85.
[29] Y. Assaf, A. Mayk, Y. Cohen, Displacement imaging of spinal cord using q-space diffusion-weighted MRI, Magn. Reson. Med. 44 (2000) 713–722.
[30] Y. Assaf, D. Ben-Bashat, J. Chapman, S. Peled, I.E. Biton, M. Kafri, Y. Segev, T. Hendler, A.D. Korczyn, M. Graif, Y. Cohen, High b-value q-space analyzed diffusion-weighted MRI: application to multiple sclerosis, Magn. Reson. Med. 47 (2002) 115–126.
[31] I.E. Biton, I.D. Duncan, Y. Cohen, Q-space diffusion of myelin-deficient spinal cords, Magn. Reson. Med. 58 (2007) 993–1000.
[32] A. Bar-Shir, Y. Cohen, High b-value q-space diffusion MRS of nerves: structural information and comparison with histological evidence, NMR Biomed. 21 (2008) 165–174.
[33] S. Peled, D.G. Cory, S.A. Raymond, D.A. Kirschner, F.A. Jolesz, Water diffusion, T-2, and compartmentation in frog sciatic nerve, Magn. Reson. Med. 42 (1999) 911–918.
[34] C. Beaulieu, The basis of anisotropic water diffusion in the nervous system—a technical review, NMR Biomed. 15 (2002) 435–455.
[35] C. Malmborg, M. Sjobeck, S. Brockstedt, E. Englund, O. Soderman, D. Topgaard, Mapping the intracellular fraction of water by varying the gradient pulse length in q-space diffusion MRI, J. Magn. Reson. 180 (2006) 280–285.
[36] J. Ellegood, R.T. Mckay, C.C. Hanstock, C. Beaulieu, Anisotropic diffusion of metabolites in peripheral nerve using diffusion weighted magnetic resonance spectroscopy at ultra-high field, J. Magn. Reson. 184 (2007) 20–28.
[37] P.J. Basser, J. Mattiello, D. Lebihan, Estimation of the effective self-diffusion tensor from the NMR spin-echo, J. Magn. Reson. B 103 (1994) 247–254.
[38] D.G. Cory, A.N. Garroway, J.B. Miller, Applications of spin transport as a probe of local geometry, Polym. Preprints 31 (1990) 149.
[39] P.T. Callaghan, M.E. Komlosh, Locally anisotropic motion in a macroscopically isotropic system: displacement correlations measured using double pulsed gradient spin-echo NMR, Magn. Reson. Chem. 40 (2002) S15–S19.
[40] M.E. Komlosh, F. Horkay, R.Z. Freldlin, U. Nevo, Y. Assaf, P.J. Basser, Detection of microscopic anisotropy in gray matter and in a novel tissue phantom using double Pulsed Gradient Spin Echo MR, J. Magn. Reson. 189 (2007) 38–45.
[41] M.E. Komlosh, M.J. Lizak, F. Horkay, R.Z. Freidlin, P.J. Basser, Observation of microscopic diffusion anisotropy in the spinal cord using double-pulsed gradient spin echo MRI, Magn. Reson. Med. 59 (2008) 803–809.
[42] E. Özarslan, P.J. Basser, Microscopic anisotropy revealed by NMR double pulsed field gradient experiments with arbitrary timing parameters, J. Chem. Phys. 128 (2008) 154511.
[43] E. Özarslan, N. Shemesh, P.J. Basser, A general framework to quantify the effect of restricted diffusion on the NMR signal with applications to double pulsed field gradient NMR experiments, J. Chem. Phys. 130 (2009) 104702.
[44] N. Shemesh, E. Özarslan, P.J. Basser, Y. Cohen, Measuring small compartmental dimensions using low-q angular double-PGSE NMR: the effect of experimental parameters on signal decay, J. Magn. Reson. 198 (2009) 15–23.
[45] P.T. Callaghan, C.H. Arns, P. Galvosas, M.W. Hunter, Y. Qiao, K.E. Washburn, Recent Fourier and Laplace perspectives for multidimensional NMR in porous media, Magn. Reson. Imaging 25 (2007) 441–444.
[46] P. Galvosas, Y. Qiao, M. Schonhoff, P.T. Callaghan, On the use of 2D correlation and exchange NMR spectroscopy in organic porous materials, Magn. Reson. Imaging 25 (2007) 497–500.
[47] P.T. Callaghan, I. Furo, Diffusion–diffusion correlation and exchange as a signature for local order and dynamics, J. Chem. Phys. 120 (2004) 4032–4038.
[48] A. Jerschow, N. Muller, Suppression of convection artifacts in stimulated-echo diffusion experiments. Double-stimulated-echo experiments, J. Magn. Reson. 125 (1997) 372–375.
[49] B. Blumich, P.T. Callaghan, R.A. Damion, S. Han, A.A. Khrapitchev, K.J. Packer, S. Stapf, Two-dimensional NMR of velocity exchange: VEXSY and SERPENT, J. Magn. Reson. 152 (2001) 162–167.
[50] E. Özarslan, P.J. Basser, MR diffusion–"diffraction" phenomenon in multi-pulse-field-gradient experiments, J. Magn. Reson. 188 (2007) 285–294.
[51] N. Shemesh, Y. Cohen, The effect of experimental parameters on the signal decay in double-PGSE experiments: negative diffractions and enhancement of structural information, J. Magn. Reson. 195 (2008) 153–161.
[52] P.P. Mitra, Multiple wave-vector extensions of the NMR pulsed-field-gradient spin-echo diffusion measurement, Phys. Rev. B 51 (1995) 15074–15078.
[53] E.G. Novikov, D. van Dusschoten, H. Van As, Modeling of self-diffusion and relaxation time NMR in multi-compartment systems, J. Magn. Reson. 135 (1998) 522–528.
[54] L. van der Weerd, S.M. Melnikov, F.J. Vergeldt, E.G. Novikov, H. Van As, Modelling of self-diffusion and relaxation time NMR in multicompartment systems with cylindrical geometry, J. Magn. Reson. 156 (2002) 213–221.
[55] C.S. Johnson, Diffusion ordered nuclear magnetic resonance spectroscopy: principles and applications, Prog. Nucl. Magn. Reson. Spectrosc. 34 (1999) 203–256.
[56] P.T. Callaghan, Principles of nuclear magnetic resonance microscopy, Oxford University Press, 1991.
[57] D.S. Grebenkov, NMR survey of reflected Brownian motion, Rev. Mod. Phys. 79 (2007) 1077–1137.
[58] E. Özarslan, Compartment shape anisotropy (CSA) revealed by double pulsed field gradient MR, J. Magn. Reson. 199 (2009) 56–67.
[59] D. Topgaard, O. Söderman, Experimental determination of pore shape and size using q-space NMR microscopy in the long diffusion time limit, Magn. Reson. Imaging 21 (2003) 69–76.
[60] J. Finsterbusch, M.A. Koch, A tensor approach to double wave vector diffusion-weighting experiments on restricted diffusion, J. Magn. Reson. 195 (2008) 23–32.
[61] M.A. Koch, J. Finsterbusch, Compartment size estimation with double wave vector diffusion-weighted Imaging, Magn. Reson. Med. 60 (2008) 90–101.
[62] T. Weber, C.H. Ziener, T. Kampf, V. Herold, W.R. Bauer, P.M. Jakob, Measurement of apparent cell radii using a multiple wave vector diffusion experiment, Magn. Reson. Med. 61 (2009) 1001–1006.